

Simple fabrication and characteristics of $Zn_2Ti_3O_8$ one-dimensional nanostructures

Sang Won Nam^a, Yong Jung Kwon^b, Hong Yeon Cho^b, Sung Yong Kang^b, Han Gil Na^b and Hyoun Woo Kim^{b,*}

^aDepartment of Electronic Engineering, Hanyang University, Seoul 133-791, Republic of Korea

^bDepartment of Materials Science and Engineering, Hanyang University, Seoul 133-791, Republic of Korea

For the first time, we report the fabrication of one-dimensional (1D) nanostructures of $Zn_2Ti_3O_8$. We heated the TeO_2/TiO_2 core-shell nanowires in a Zn-containing environment. The variation in heating temperature drastically changed the morphology and structure of the composite nanowires, obtaining the 1D nanostructures of $Zn_2Ti_3O_8$ at 700 °C. A photoluminescence (PL) study indicated that annealing at 700 °C generated a PL band at 2.5 eV in the green region, originating from the $Zn_2Ti_3O_8$ structure. These findings may pave the way to fabrication and applications of novel composite nanostructures.

Key words: $Zn_2Ti_3O_8$, Nanostructures, Photoluminescence.

Introduction

Zinc titanates have been used as attractive sorbents for removing sulfur from hot coal gasification products [1, 2]. They have also been used as dielectric resonators and filters [3, 4]. Similarly, Kim et al. indicated that zinc titanates can be used as a dielectric material for microwave devices [5, 6].

Zinc titanates are known to crystallize in three common forms: Zn_2TiO_4 (face-centered cubic), $Zn_2Ti_3O_8$ (cubic), and $ZnTiO_3$ (hexagonal). Among them, $Zn_2Ti_3O_8$ has a higher Ti content, having a better lithium anode composition than other zinc titanates [7]. Accordingly, $Zn_2Ti_3O_8$ is a strong candidate for an anode material in a rechargeable lithium-ion battery [7].

In spite of its scientific and technological importance, it is very difficult to form $Zn_2Ti_3O_8$ because it is a metastable phase. $Zn_2Ti_3O_8$ tends to decompose into $ZnTiO_3$ and TiO_2 phases when heated to 800 °C [8, 9]. Datta has revealed that $Zn_2Ti_3O_8$ does not exist in a stable phase but only forms as a metastable transition phase when ZnO reacts with anatase TiO_2 [10]. While Zn_2TiO_4 and $ZnTiO_3$ are the most common forms and have been intensively studied, $Zn_2Ti_3O_8$ is a metastable phase that is the most difficult to form [7]. The existence of a metastable $Zn_2Ti_3O_8$ phase was first reported by Bartrasm and Slepetyts [11]. $Zn_2Ti_3O_8$ is composed of octahedral $[TiO_6]$ and tetrahedral $[ZnO_4]$, as shown in Hong et al.'s work [7]. Steinke et al. reported that $Zn_2Ti_3O_8$ can be described by the spinel formula, which can provide unoccupied sites [12].

Nanostructures are attracting great attention due to

their novel physical properties [13-32], and one-dimensional (1D) nanostructured materials including nanorods, nanowires, and nanotubes are also receiving considerable attention owing to their remarkable physical properties and potential applications.

In the present work, we have successfully fabricated 1D nanostructures of $Zn_2Ti_3O_8$ for the first time. Core TeO_2 nanowires were prepared by a simple heating method. Next, we coated the core nanowires with ZnO layers by means of the atomic layer deposition (ALD) technique. Finally, the core-shell nanowires were annealed in ambient air at temperatures ranging from 500-900 °C. We found that the annealing temperature significantly affected the composition and morphology of the resulting product. In particular, we have produced pseudo-nanotubes of the $Zn_2Ti_3O_8$ phase by annealing at 700 °C. Although pseudo-nanotubes are only partially-vacant nanotubes, they have the potential to attract great interest not only due to their superior optical, electrical, thermal, and mechanical properties, but also because of their efficiency and activity caused by their high porosity and large surface area [33]. Furthermore, we have characterized samples in terms of both their structure and photoluminescence (PL).

Experimental

Core TeO_2 nanowires were prepared by heating the source Te powders in a high-temperature vertical tube furnace in N_2 ambient at a flow rate of 2 standard liters per min (slm). A schematic diagram of the experimental apparatus was reported in [34]. Te powder (99.9% purity) was used as the source material. Si plate coated with a 3 nm Au layer was used as the substrate for collecting the growth products. The temperature of substrate was set to 400 °C in a nitrogen

*Corresponding author:
Tel : +82-2-2220-0382
Fax: +82-2-2220-0389
E-mail: hyounwoo@hanyang.ac.kr

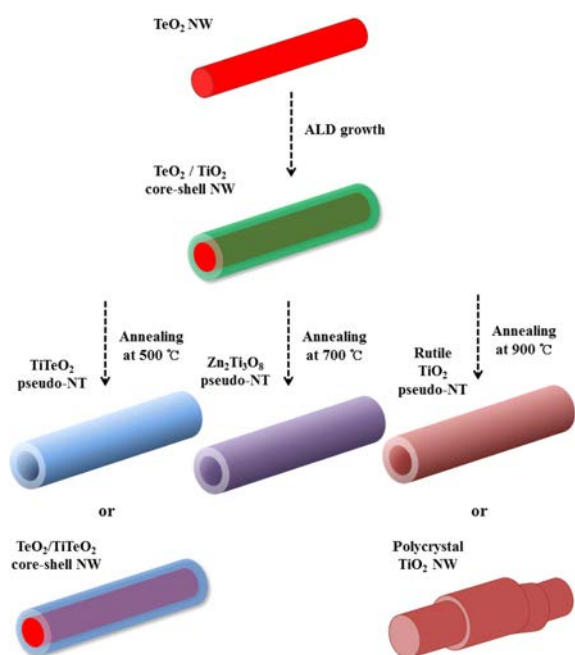


Fig. 1. Schematic outline of the process sequence for the generation of 1D nanostructures at 500, 700, and 900 °C.

(N₂) gas flow, in which the gas flow rate was 2 standard liters per min (slm).

We carried out the ALD of the TiO₂ shell layers on the core TeO₂ nanowires using tetrakis(dimethylamino) titanium (TDMAT) and a mixture of O₃/O₂ as the Ti and O precursors, respectively. The TDMAT bubbler was maintained at 40 °C. The injection time of TDMAT was 5 s, which was divided into two periods: The first period is the sourcing step without the carrier gas for 1 s. The second period delivers the Ar gas with a flow rate of 100 sccm for 4 s. Since the surface sites become saturated with the precursor in the ALD process, the subsequent purging removes the excess precursor, which was not mono-atomically attached to the surface. A mixture of O₃ and O₂ was pulsed for 2 s to oxidize the chemisorbed metal precursor. Then, an Ar-purge was carried out for 5 s, with an Ar flow rate of 400 sccm. The number of ALD cycles and the substrate temperature were set to 500 and 300 °C, respectively. Subsequently, the core-shell nanowires were thermally annealed with staples (No. 33, Peace Korea Ltd.) in a mixture of Ar and air gases (percentage of the air partial pressure of 3%) at temperatures ranging from 500-900 °C. We found that the Zn vapors originate from the surface of the staples (According to Peace Korea Ltd., the staple consists of a Fe-core/Zn-shell). In the heating process, the pressure was maintained at less than 2 Torr by using a rotary pump. Fig. 1 describes the process sequences of the fabrication of nanostructures at various temperatures.

Scanning electron microscopy (SEM) images were acquired using a Hitachi S-4200. Glancing angle (0.5 °) X-ray diffraction (XRD) was carried out using a

Philips X'pert MPD system with CuK α ₁ radiation. Transmission electron microscopy (TEM) and energy-dispersive X-ray (EDX) spectroscopy were carried out using a Philips CM 200 operating at 200 kV. The PL spectra were acquired at room temperature on a SPEX-1403 photoluminescence spectrometer using a 325 nm line from a He-Cd laser (Kimon, Japan).

Results and Discussion

Fig. 2(a) shows the XRD spectrum of the as-prepared TeO₂ nanowires, while Fig. 2(b)-2(d) corresponds to the XRD spectra of the TiO₂-shelled TeO₂ nanowires. In the case of Fig. 2(b), (c), and (d), the core-shell nanowires were annealed at temperatures of 500, 700, and 900 °C, respectively. The XRD spectra of the as-prepared TeO₂ nanowires contain a variety of TeO₂-related phases, including tetragonal TeO₂ (JCPDS Card: 42-1365), orthorhombic γ -TeO₂ (JCPDS Card: 52-1005), and orthorhombic TeO₂ (JCPDS Card: 76-0680). By means of annealing at 500 °C, besides the TeO₂-associated phases, diffraction peaks with respect to the tetragonal TiO₂ (Lattice constants $a = 4.5933\text{Å}$

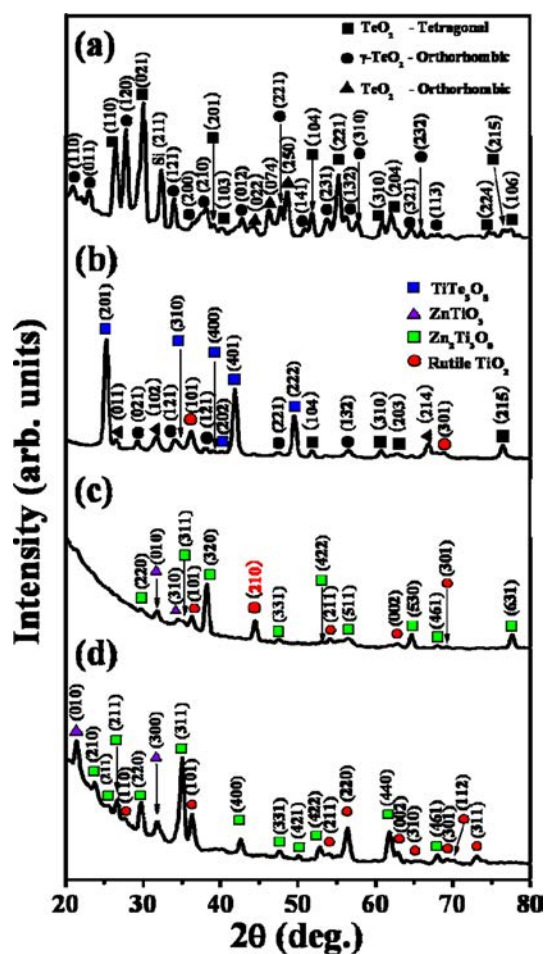


Fig. 2. (a) XRD pattern of the as-synthesized TeO₂ nanowires. XRD patterns of the TeO₂/TiO₂ core-shell nanowires annealed at (b) 500, (c) 700, and (d) 900 °C.

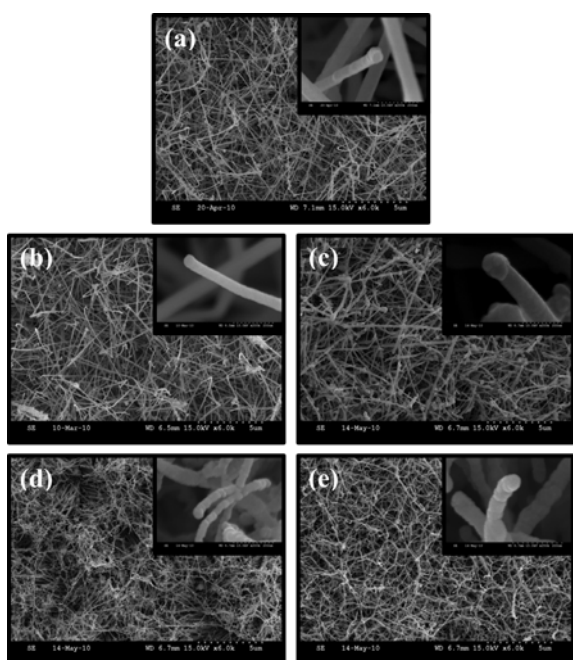


Fig. 3. SEM images of the (a) as-synthesized and (b) TiO_2 -coated TeO_2 nanowires. SEM images of the TeO_2/TiO_2 core-shell nanowires annealed at (c) 500, (d) 700, and (e) 900 °C.

and $c = 2.9592\text{\AA}$; JCPDS No. 21-1276) and hexagonal $TiTe_3O_8$ (Lattice constants $a = 10.764\text{\AA}$ and $c = 5.142\text{\AA}$; JCPDS No. 41-0076). Furthermore, by annealing at 700 °C, the XRD spectrum changed considerably. Fig. 2(c) shows that the diffraction peaks can be assigned not only to the rutile TiO_2 phase, but also to the $Zn_xTi_yO_z$ -related phases. In this case, the $Zn_xTi_yO_z$ -related phases were comprised of cubic $ZnTiO_3$ with a lattice constant of $a = 8.408\text{\AA}$ (JCPDS No. 39-0290) and cubic $Zn_2Ti_3O_8$ with a lattice constant of $a = 8.392\text{\AA}$ (JCPDS No. 87-1781). Being similar to the 700 °C annealed sample, the XRD spectrum of the 900 °C annealed sample exhibited diffraction peaks corresponding to rutile TiO_2 , cubic $ZnTiO_3$, and cubic $Zn_2Ti_3O_8$. SEM investigation revealed that the 1D morphology of the TeO_2 nanowires did not change from either the TiO_2 coating or the subsequent thermal annealing (Fig. 3).

In order to investigate the structure, composition, and crystallinity of the 700 °C annealed sample, we carried out a TEM characterization. Fig. 4(a) shows a TEM image of the 1D nanostructure. Fig. 4(b) shows a lattice-resolved TEM image. The marked interplanar spacings of 0.21, 0.25, 0.35, and 0.36 nm correspond to the (400), (311), (211), and (210) lattice planes of cubic $Zn_2Ti_3O_8$. The corresponding SAED pattern is depicted in Fig. 4(c). Ring patterns corresponding to the {210}, {211}, {220}, {311}, and {400} lattice planes of cubic $Zn_2Ti_3O_8$ are clearly observed, revealing a polycrystalline nature. Fig. 5 shows the EDX spectrum of the 700 °C annealed sample, indicating the presence of C, Cu, O, Zn, and Ti elements. Since the C and Cu elements are

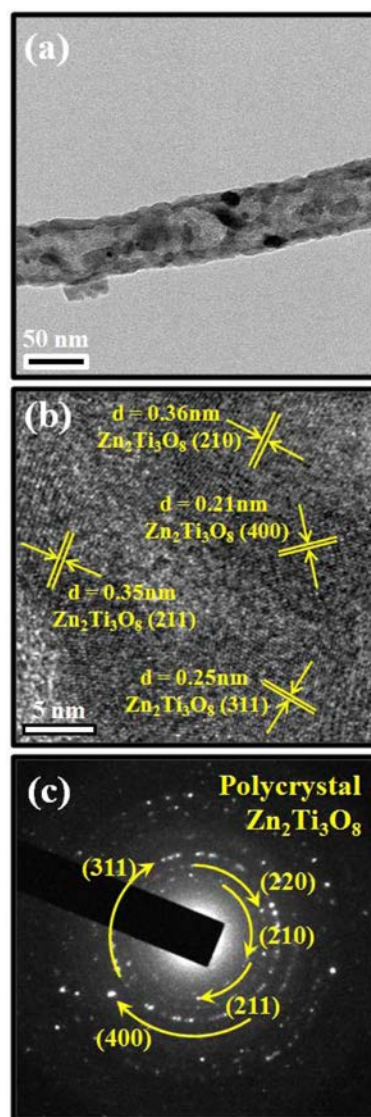


Fig. 4. (a) Low-magnification TEM image, (b) lattice-resolved TEM image, and (c) SAED pattern of the TeO_2/TiO_2 core-shell nanowires annealed at 700 °C.

supposed to originate from the C-coated Cu grid, the 700 °C annealed sample is comprised of Zn, Ti, and O elements.

The EDX line scan along the diameter of the $Zn_2Ti_3O_8$ 1D structures reveals that the amount of Te element is negligible compared to those of the Zn, Ti, and O elements (Fig. 6). Furthermore, the Zn, Ti, and O line scans exhibit slight valley-like profiles. If the structures were to be perfect solid ones, the profiles would have exhibited a convexed shape. Therefore, we surmise that the nanowires have a pseudo-tube-like morphology.

TEM investigation for the 900 °C annealed samples was also carried out. Fig. 7(a) shows a TEM image of the 900 °C annealed nanowires. The diameter was estimated to be about 44–71 nm. Fig. 7(b) shows a lattice-resolved TEM image enlarging the squared area

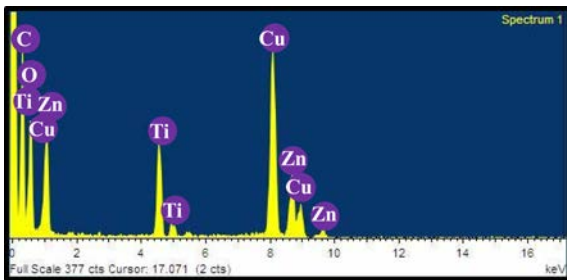


Fig. 5. EDX spectrum of the $\text{TeO}_2/\text{TiO}_2$ core-shell nanowires annealed at 700°C .

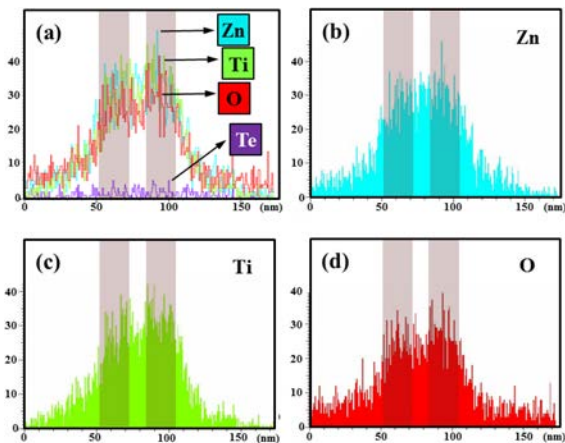


Fig. 6. EDX line scan along the diameter of the $\text{Zn}_2\text{Ti}_3\text{O}_8$ 1D structures synthesized at 700°C . (a) Overlapped graph for the Zn, Ti, O, and Te elements. Individual scans for the (b) Zn, (c) Ti, and (d) O elements.

in Fig. 7(a). The interplanar distances were measured to be about 0.25 and 0.32 nm, corresponding to the (101) and (110) planes of the tetragonal TiO_2 (JCPDS No. 21-1276). It is noteworthy that the nanowire is polycrystalline, consisting of TiO_2 -phased grains. Fig. 7(c) shows the associated SAED pattern, confirming that the nanowire is comprised of many TiO_2 -phased grains.

Fig. 8 shows the results of the EDX investigation for the $\text{TeO}_2/\text{TiO}_2$ core-shell nanowires annealed at 900°C . The individual elemental maps reveal that the Ti and O elements are clearly visible, whereas the Te and Zn elements are invisible. However, the XRD results shown in Fig. 2d indicate that there is not only a TiO_2 phase, but there are also cubic ZnTiO_3 and cubic $\text{Zn}_2\text{Ti}_3\text{O}_8$ phases. Accordingly, we surmise that the 900°C -grown nanostructure is mainly comprised of a TiO_2 phase. In addition, the ZnTiO_3 and $\text{Zn}_2\text{Ti}_3\text{O}_8$ phases are deposited on the substrate, not in the 1D nanostructures. Secondly, it is possible that a small amount of ZnTiO_3 and $\text{Zn}_2\text{Ti}_3\text{O}_8$ phases are located in the 1D structures. From the thermodynamics, $\text{Zn}_2\text{Ti}_3\text{O}_8$ decomposes into ZnTiO_3 and TiO_2 phases when heated to 800°C [8, 9]. In the present work, the $\text{Zn}_2\text{Ti}_3\text{O}_8$ structures, which are stable at 700°C decompose into ZnTiO_3 and TiO_2 phases. The TiO_2 phase will likely become a major

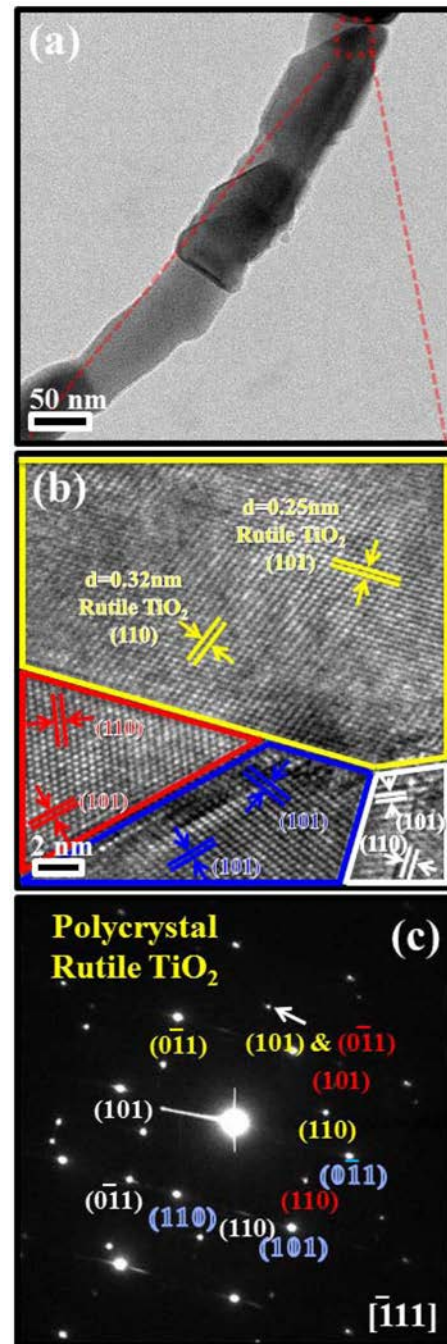


Fig. 7. (a) Low-magnification TEM image of the $\text{TeO}_2/\text{TiO}_2$ core-shell nanowires annealed at 900°C . (b) Lattice-resolved TEM image enlarging the squared region in (a). (c) Corresponding SAED pattern.

constituent of 900°C grown nanostructures. Further detailed study will be conducted later.

In a previous paper, we fabricated nanotubes by preparing core-shell nanowires and subsequently removing the core TeO_2 nanowires [35]. We surmise that the core TeO_2 nanowires can be removed efficiently by thermal heating, due to the activation of the vaporization of solid TeO_2 [36]. The vapor pressures of TeO_2 at 500°C , 700°C , and 900°C were 3.60×10^{-8} , 5.85×10^{-5} , and 7.36×10^{-3} atm

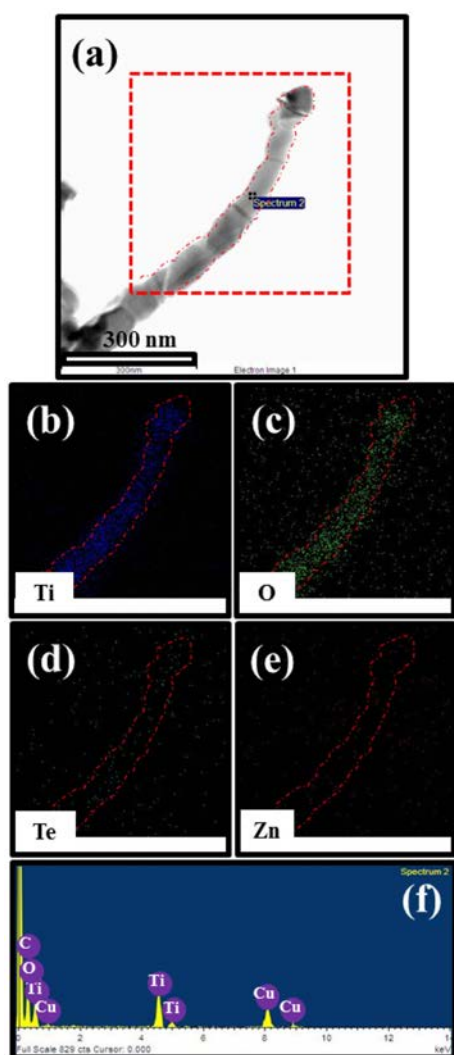


Fig. 8. (a) Typical TEM image of the $\text{TeO}_2/\text{TiO}_2$ core-shell nanowires annealed at 900°C . (b) EDX spectrum and elemental maps for the (c) Ti, (d) O, (e) Te, and (f) Zn elements.

[37], respectively, suggesting a drastic increase in the TeO_2 vapor pressure at higher temperatures.

The evaporation of TeO_2 nanowires at temperatures considerably lower than the boiling temperature (1245°C) was due to the size effect, in which the evaporation temperature of the nanocrystals was found to be size-dependent and decreases with decreasing size, i.e., the diameter of the nanoparticles and nanorods, or the thickness of the thin films [38]. Although it is not shown in this paper, TGA analysis indicated that the evaporation of the TeO_2 nanotubes occurred at about 816°C , which is considerably lower than their boiling temperature (1245°C) [35]. Furthermore, under a lower ambient pressure of < 2 Torr in the present work, TeO_2 is supposed to evaporate at a lower temperature [35].

Fig. 9 shows the PL spectra of various samples measured at room temperature. The PL spectrum of the uncoated TeO_2 nanowires corresponds to the band centered at approximately 2.8 eV in the blue region

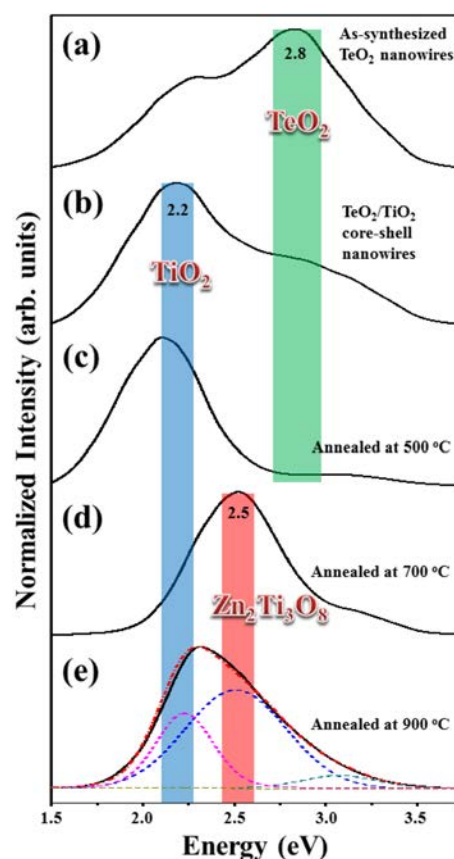


Fig. 9. PL spectra of the (a) TeO_2 nanowires and (b-e) $\text{TeO}_2/\text{TiO}_2$ core-shell nanowires, which were (b) as-fabricated, (c) 500°C -annealed, (d) 700°C -annealed, and (e) 900°C -annealed.

in Fig. 9(a). A similar blue band has been observed with TeO_2 crystals, which is due to the radiative recombination of self-trapped excitons [39, 40]. Fig. 9(b) shows the PL spectrum of the as-synthesized $\text{TeO}_2/\text{TiO}_2$ core-shell nanowires. The PL spectrum is comprised of two emission bands peaked at approximately 2.2 eV (yellow-green) and 2.8 eV (blue), respectively. While the 2.8 eV -band is related to the TeO_2 structures, the 2.2 eV -band is associated with the TiO_2 structure. The 2.2 eV -band presumably originates from the charge-transfer transition from Ti^{3+} to an oxygen anion in a TiO_6^{8-} complex [41].

Fig. 9(c) shows the PL spectrum of the $\text{TeO}_2/\text{TiO}_2$ core-shell nanowires, which were annealed at 500°C . By comparing Fig. 9(c) with Fig. 9(b), we observe that the blue emission band has been significantly suppressed. Based on the XRD results (Figs. 2(a) and 2(b)), we suggest that the suppression of the blue band is related to the disappearance of the TeO_2 structure by thermal annealing. Fig. 9(d) shows the PL spectrum of the $\text{TeO}_2/\text{TiO}_2$ core-shell nanowires, which were annealed at 700°C . XRD and TEM analyses reveal that the 700°C annealed nanowires mainly consist of a cubic $\text{Zn}_2\text{Ti}_3\text{O}_8$ structure. Accordingly, we suppose that the 2.5 eV -band in the green region mainly originates from the $\text{Zn}_2\text{Ti}_3\text{O}_8$ structure. Similarly, the $\text{Zn}_2\text{Ti}_3\text{O}_8$ structure exhibits a

green emission, presumably due to the oxygen vacancies [42].

Fig. 9(e) shows the PL spectrum of the TeO₂/TiO₂ core-shell nanowires, which were annealed at 900 °C. In terms of the Gaussian fitting analysis, the PL spectrum was deconvoluted into two primary emission bands at approximately 2.2 eV (yellow-green) and 2.5 eV (blue), respectively. By comparing Fig. 9(d) with Fig. 9(e), we observe that the blue emission band appears by means of the increase in the annealing temperature from 700 to 900 °C. This observation coincides with the TEM results showing that the 900 °C annealed nanostructure is mainly comprised of a tetragonal TiO₂ phase. In addition, the 2.5 eV band in the green region is associated with a Zn₂Ti₃O₈ or ZnTiO₃ structure.

Conclusions

For the first time, we have successfully fabricated 1D nanostructures of cubic Zn₂Ti₃O₈. Through fabrication by coating TiO₂ shell layers on core TeO₂ nanowires by ALD, we heated the TiO₂-coated TeO₂ nanowires in a range of 500-900 °C. While the composite nanowires maintain a 1D morphology irrespective of the annealing temperature, their composition and structure have been significantly changed. Surprisingly, the 500 °C annealed nanostructure exhibits the existence of a hexagonal TiTe₃O₈ phase. By means of the lattice-resolved TEM, SAED pattern, and EDX spectrum, the 700 °C annealed nanostructure turned out to be a pseudo-nanotube, mainly consisting of a cubic Zn₂Ti₃O₈ phase. The lattice-resolved TEM, SAED pattern, and EDX spectrum coincidentally indicate that the 900 °C annealed nanostructure corresponds to the solid nanowires or the pseudo-nanotubes, which are mainly comprised of a tetragonal rutile TiO₂ phase. The room-temperature PL spectra confirmed that the 2.8 eV and 2.2 eV bands originated from the TeO₂ and TiO₂ phases, respectively. The annealing at 500 °C suppressed the 2.8 eV band, coinciding with the XRD results showing that the TeO₂ phase evaporated. The annealing at 700 °C generated a 2.5 eV band, representing the appearance of a cubic Zn₂Ti₃O₈ phase. Higher-temperature annealing at 900 °C generated a TiO₂ phase, indicating a reduction of the Zn₂Ti₃O₈ phase.

Acknowledgments

This work was supported by a National Research Foundation of Korea (NRF) grant funded by the Korean government (MEST) (No. NRF-2013R1A2A2 A01068438).

References

1. J. H. Swisher and K. Schwerdtfeger, *J. Mater. Eng. Perform.* 1 (1992) 565-571.

2. J. H. Swisher, J. Yang and R. P. Gupta, *Ind. Eng. Chem. Res.* 34 (1995) 4463-4471.

3. H. Kagata, T. Inoue, J. Kato, I. Kameyama and T. Ishizaki, *Ceram. Trans.* 32 (1993) 81-90.

4. T. Negas, T. Yeager, S. Bell and N. Coats, *Am. Ceram. Soc. Bull.* 72 (1993) 80-89.

5. H. T. Kim, J. D. Byun and Y. Kim, *Mater. Res. Bull.* 33 (1998) 963-973.

6. H. T. Kim, J. D. Byun and Y. Kim, *Mater. Res. Bull.* 33 (1998) 975-986.

7. Z. Hong, M. Wei, Q. Deng, X. Ding, L. Jiang and K. Wei, *Chem. Commun.* 46 (2010) 740-742.

8. J. Yang and J. H. Swisher, *Mater. Char.* 37 (1996) 153-159.

9. Y.-L. uang, D.-C. Tsai, Y.-C. Lee, D.-R. Jung and F.-S. Shieu, *Surf. Coat. Technol.* 231 (2013) 153-156.

10. R. K. Datta, in "Composition modification and characterization of ZnO-TiO₂ based (ZTB) desulfurization sorbents" (Final Report under U.S. department of energy, 1993).

11. S. F. Bartram and R. A. Slepetyts, *J. Am. Ceram. Soc.* 44 (1961) 493-499.

12. U. Steinike and B. Wallis, *Cryst. Res. Technol.* 32 (1997) 187-193.

13. R. Kuar, M. C. Mishra, B. K. Sharma, V. Vyas and G. Sharma, *Electron. Mater. Lett.* 9 (2013) 19-23.

14. H.-W. Cui, D.-S. Li and Q. Fan, *Electron. Mater. Lett.* 9 (2013) 1-5.

15. M. A. Majeed Khan, W. Khan, M. Ahamed, M. S. Alsalthi and T. Ahmed, *Electron. Mater. Lett.* 9 (2013) 53-57.

16. R. Sabbaghizadeh and M. Hashim, *Electron. Mater. Lett.* 9 (2013) 115-118.

17. D. Soundararajan, Y. Lim, M.-P. Chen and K. H. Kim, *Electron. Mater. Lett.* 9 (2013) 177-182.

18. T. Prakash, S. Ramasamy and B. S. Murty, *Electron. Mater. Lett.* 9 (2013) 207-211.

19. A. Mondal, J. C. Dhar, P. Chinnamuthu, N. K. Singh, K. K. Chattopadhyay, S. K. Das, S. Ch Das and A. Bhattachayya, *Electron. Mater. Lett.* 9 (2013) 213-217.

20. S. N. Heo, K. Y. Park, Y. J. Seo, F. Ahmed, M. S. Anwar and B. H. Koo, *Electron. Mater. Lett.* 9 (2013) 261-265.

21. S. Sharma and S. Chawla, *Electron. Mater. Lett.* 9 (2013) 267-271.

22. K. Seo, M. Suh and S. Ju, *Electron. Mater. Lett.* 9 (2013) 273-277.

23. C.-H. Lee, D.-J. Choi and Y.-J. Oh, *Electron. Mater. Lett.* 9 (2013) 283-286.

24. Y. Jia, F. Yang, F. Cai, C. Cheng and Y. Zhao, *Electron. Mater. Lett.* 9 (2013) 287-291.

25. S. Kim, G. Nam, K. G. Yim, J. Lee, Y. Kim and J.-Y. Leem, *Electron. Mater. Lett.* 9 (2013) 293-298.

26. H.-W. Cui, D.-S. Li and Q. Fan, *Electron. Mater. Lett.* 9 (2013) 299-307.

27. H. Lee, J.-H. Shin, J. Chae, J. B. Kim, T.-H. Kim and K.-B. Park, *Electron. Mater. Lett.* 9 (2013) 357-362.

28. S. Kumar, P. Dharma and V. Sharma, *Electron. Mater. Lett.* 9 (2013) 371-374.

29. T. Sreesattabud, B. J. Gibbons, A. Watcharapasom and S. Jansirisomboon, *Electron. Mater. Lett.* 9 (2013) 409-412.

30. N.-M. Park, J. Shin, B. Kim, K. H. Kim and W.-S. Cheong, *Electron. Mater. Lett.* 9 (2013) 467-469.

31. C.-G. Kuo, H. Chang, L.-R. Hwang, S. Hor, J.-S. Chen, G.-Y. Liu and S.-C. Cheng, *Electron. Mater. Lett.* 9 (2013) 481-484.

32. J. Huang, S. Somu and A. Busnaina, *Electron. Mater. Lett.* 9 (2013) 505-507.

33. J. J. Wu, S. C. Liu, C. T. Wu, K. H. Chen and L. C. Chen, *Appl. Phys. Lett.* 81 (2002) 1312.
34. N. H. Kim and H. W. Kim, *Appl. Phys. A* 80 (2005) 537-540.
35. H. W. Kim, H. G. Na and J. C. Yang, *Chem. Eng. J.* 170 (2011) 326-332.
36. D. W. Muenow, J. W. Hastie, R. Hauge, R. Bautista and J. L. Margrave, *Trans. Faraday Soc.* 65 (1969) 3210-3220.
37. S. Balakrishnan, R. Pankajavalli, K. Ananthasivan and S. Anthonysamy, *Thermochim. Acta* 467 (2007) 80-85.
38. K. K. Nanda, *Appl. Phys. Lett.* 87 (2005) 021909.
39. I. Dafinei, M. Diemoz, E. Longo, A. Peter and I. Földvari, *Nucl. Instrum. Meth. A* 554 (2005) 195-200.
40. I. Dafinei, C. Dujardin, E. Longo and M. Vignati, *Phys. Stat. Sol. (a)* 204 (2007) 1567-1570.
41. J. C. Yu, J. Yu, W. Ho, Z. Jiang and L. Zhang, *Chem. Mater.* 14 (2002) 3808-3816.
42. 42X. Qin, L. Cui and G. Shao, *J. Nanomater.* 2013 (2013) 428419.